Soft Matter

View Online
Dynamic Article Links

Cite this: DOI: 10.1039/c1sm05565h

www.rsc.org/softmatter

PAPER

Electrorheological response of dense strontium titanyl oxalate suspensions

Carlos S. Orellana, Jinbo He and Heinrich M. Jaeger*

Received 1st April 2011, Accepted 3rd June 2011
DOI: 10.1039/c1sm05565h

In suspensions of polarizable particles the addition of polar molecules can dramatically increase the yield stress under an applied electric field, leading to a giant electrorheological (GER) effect. We report experiments on dense suspensions of strontium titanyl oxalate in silicon oil, where we find a yield stress of up to 200kPa at 5kV/mm. The magnitude of this yield stress directly correlates with the water content in the particles. In the dynamic response we observe behavior not previously reported for GER fluids and similar to sheared granular materials, including a direct proportionality between shear and normal stresses and the creation of a shear band a few particles in width. An important consequence is that the dynamic response can be varied dramatically by changing the confinement of the suspension or by imposing a normal stress.

1. Introduction

Electrorheological (ER) fluids consist of highly polarizable micron- or nano-size particles dispersed in an insulating liquid (typically an oil).[1–5] When an electric field is applied, the particles become polarized and align with the field, leading to the formation of system-spanning particle chains that produce a yield stress. First reported by Winslow in 1949,[6] regular ER fluids exhibit maximum strengths around 10kPa at $E = 5$kV/mm.[7] Since yield stresses of this magnitude are too small for many applications and cannot be improved significantly, ER fluids have not been used as widely as their magnetorheological counterparts.[3] In 2003, however, Wen *et al.* showed that barium titanyl oxalate particles, coated with a thin urea layer providing permanent dipoles, exhibit a dramatically increased field response, which they termed the giant electrorheological (GER) effect.[8] In this system, the particles form chains along the field direction as in the ordinary ER effect, but, with local electric fields between adjacent particles reaching 10^2–10^3E due to the high dielectric constant of the particles, the polar urea molecules also become aligned. The presence of aligned molecular dipoles in the nanometre scale gaps between particles produces yield stresses that can exceed the usual ER effect by more than one order of magnitude.[9,10] As a consequence of these dipoles, another key signature of the GER effect (also called polar-molecule-dominated electrorheological, or PM-ER, effect[9,11]) is the linear dependence of the yield stress on the applied field.[8,10,12] The combination of very large yield stresses and linear field dependence was subsequently also observed in dense suspensions of titanium dioxide, calcium titanyl oxalate and strontium titanyl oxalate particles.[11,13–16]

While the notion of molecular dipoles as the main ingredient for the GER effect is well established,[5,8,9,11,17–19] studies of the microscopic details of the mechanism are still ongoing.[10] Furthermore, there remain open questions concerning the details of the mechanical response to applied shear.[5,19] Here we focus on the relationship between (quasi-) static quantities, such as the yield stress, and the dynamic behavior at large strain. We present systematic rheological measurements on dense suspensions of strontium titanium oxalate (STO) particles in 10 cSt silicon oil. This GER material was chosen because it allows for a particularly straightforward tuning of its performance under an electric field by simply varying the water content in the STO particles; no special coating with urea or other polar molecules is required as the water provides the dipoles. Our data show that dense STO suspensions exhibit rheological behavior unlike typical field-activated fluids. Instead, a shear response is found that has many similarities to a sheared granular material, in line with recent observations on a wide range of other dense suspensions.[20,21] We demonstrate that in such systems the yielding behavior is controlled by the stress loading history and the boundary conditions. In particular, strong confinement of the suspension to counteract shear-induced dilation is found to be critical for reaching large yield stresses.

2. Experimental

To prepare the STO particles we used a synthesis that is a modified version of the method described originally by Wen and coworkers[8] for barium-based GER particles and differs from the method by Lu *et al.* in their work on STO.[13] All chemicals were purchased from Sigma-Aldrich in ACS reagent grade and used as received. Briefly, the synthesis proceeded as follows. Strontium chloride and oxalic acid were separately dissolved in pure water to concentrations of 2M and 1M, respectively. Titanium chloride was carefully hydrolyzed to a concentration of 2M

James Franck Institute and Department of Physics, The University of Chicago, 929 E 57th Street, Chicago IL, 60637, USA. E-mail: h-jaeger@uchicago.edu; Fax: +1 773 843-0406; Tel: +1 773 702-6074

by slowly adding ice. Oxalic acid solution was heated to 60 °C, sonicated and stirred when titanium chloride solution was added. After that strontium chloride solution was added. The molar ratio of strontium chloride to titanium chloride to oxalic acid was 1 : 1 : 2. The final solution was clean due to the high solubility of strontium titanyl oxalate in water at high temperatures. Ethanol (40% by volume) was added to the mixed solution to precipitate the strontium titanyl oxalate under sonication and stirring at 60 °C. The final product was cooled down, aged and washed repeatedly with ethanol/water solution (40%/60% by volume) until pH neutrality was reached. The sample was then filtered and dried under vacuum for 2 days at room temperature or until the desired water content was reached.

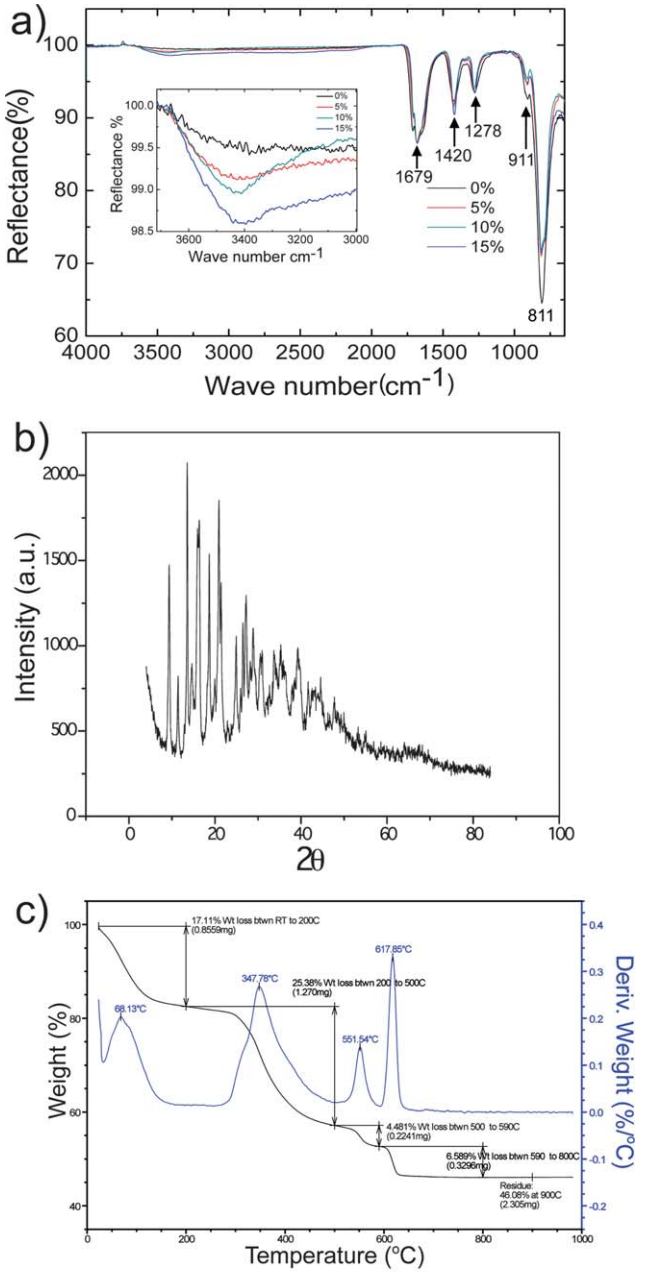

Fig. 1 Characterization of strontium-titanyl-oxalate (STO) particles. *a*) FTIR spectra for samples with different water content. Inset: Zoomed-in detail of characteristic reflectance changes associated with water content. *b*) XRD analysis reveals a semi-crystalline particle structure. *c*) Thermogravimetric data. The blue trace is the derivative of the data given by the black curve.

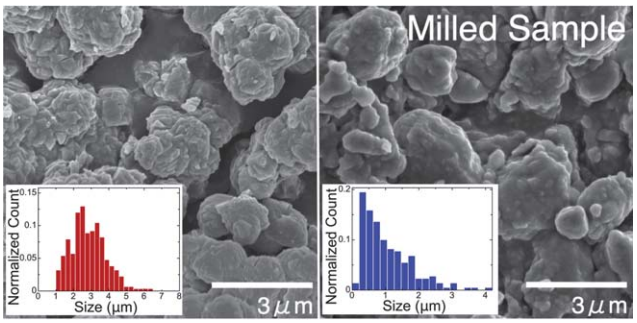

Fig. 2 Scanning electron microscope (SEM) images of STO particles before (left) and after (right) the milling process. Both insets shows histograms of particle size.

The resulting samples were characterized by Fourier transform infrared spectroscopy to confirm their composition by comparison with published STO spectra[22,23] (Fig.1a). The observed peaks at 811cm^{-1}, 911cm^{-1}, 1278cm^{-1}, 1420cm^{-1} and 1679cm^{-1} match the characteristic vibration frequencies of previously reported FTIR spectra of STO.[22] The vibration at 3400 cm^{-1} belongs to water, where a systematic change of the peak intensities is observed as the water content changes, as shown by the inset of Fig.1a. X-ray diffraction data reveals a semi-crystalline structure (Fig.1b), with a diffraction spectrum that combines broad features characteristic of the amorphous structure of barium- and strontium-based GER particles previously reported[8,13] and the sharp peaks (9.3°, 11.4°, 13.6°, 14.6°, 15.9°, 18.7°, 21°, *etc.*) from crystalline STO.[22]

A detailed thermogravimetric analysis of STO particles has been described by Fan and coworkers.[22] Each STO molecule is associated with four water molecules as the explicit chemical formula $SrTiO(C_2O_4)_2 \cdot 4(H_2O)$ shows. As temperature is increased, the two H_2O molecules with the lowest binding energy dissociate first, leading to the fast drop in water content around 68 °C (Fig.1c). The remaining water molecules are expelled by 165 °C, with a total weight loss of ~ 17%. No further weight loss is observed before 250 °C, which indicates that the chemical structure does not change. Above 300 °C, the anhydrous STO particles start to decompose into $SrCO_3$ and TiO_2 with a total weight loss of 42.4%, similar to what was observed in Ref.22. Finally, above 500 °C, the total weight loss of 53.6% indicates that $SrTiO_3$ is formed.

The STO particles were mixed with 10 cSt dry silicon oil using a high-speed ball mill (Spex Sample Prep, 8000D) in stainless steel vials for 1 h. Fig.2 shows SEM images of the particles before and after the mixing process. Before mixing the particles have a mean size close to 3μm. After mixing we find a significant increase in the fraction of smaller sizes around 300–500nm. After samples were mixed, we found them to be stable for several months.

In keeping with the previous GER literature, we report the particle concentration as the ratio of the dry STO powder by

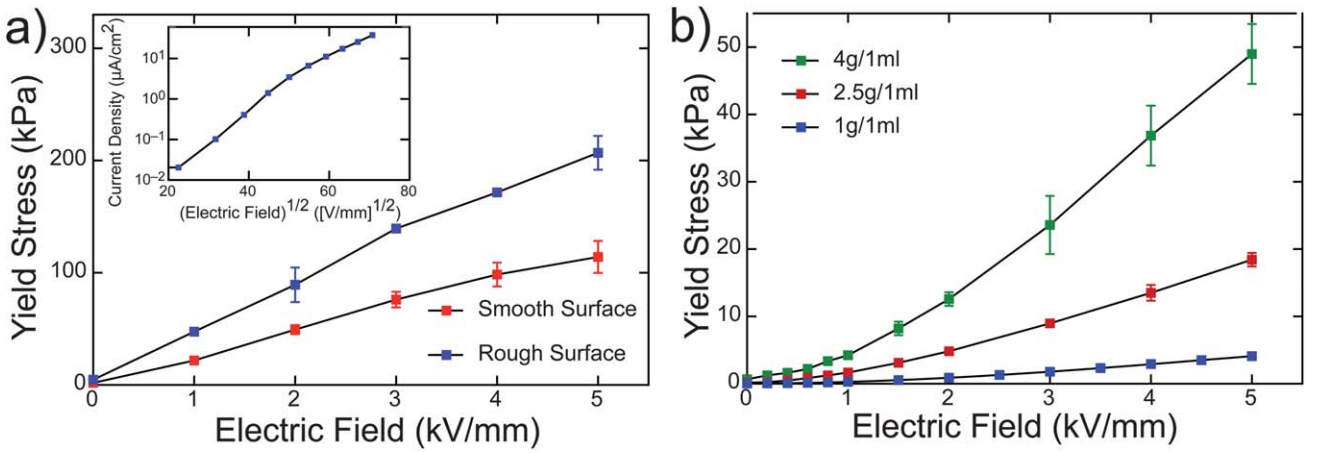

Fig. 3 *a*) Yield stress *vs.* E-field measured with different electrode surfaces (STO/oil 4g ml^{-1}; 16% water content). Inset: current density *vs.* E-field. *b*) Yield stress *vs.* E-field for different STO concentrations at 10% water content. Zero E-field yield stresses for these samples were approximately 800Pa, 80Pa and 8Pa, top to bottom.

weight before mixing to volume of oil; thus, STO/oil 4g ml^{-1} refers to a sample of 4g STO that was mixed into 1ml oil.

Stress-strain measurements were conducted with a rheometer (Anton Paar model MCR 301) with parallel-plate ER tools of diameter D = 25mm or 8 mm. Electric fields were applied between the plates using a dc power supply (Fug, model HCP 14-12500). All measurements were performed at controlled temperature 20 °C. Both stress- and shear-rate-controlled shear modes were employed, depending on the measurement. The gap separation between the electrodes was typically set to remain at a fixed value of 1mm (gap control mode) and the sides of the sample were free to expand or contract slightly in radial direction. Because there is some known, residual compliance of the ER tool in the vertical direction, variations in normal stress detected in gap control mode can be used as direct indicators of small variations in gap separation. To investigate the role of confinement we conducted a separate series of measurements in which the sample was radially confined by a non-conducting cylindrical ring and a fixed normal force was applied (normal force control mode). For large normal forces this configuration approximates the sealed Couette geometries used in clutch-type applications of ER or GER fluids.[3,24]

3. Results and discussion

We define the yield stress as the maximum of the shear stress *vs.* strain curve at a given, fixed shear rate $\dot{\gamma}$; unless noted we take $\dot{\gamma} = 0.1\text{s}^{-1}$.† Fig.3a shows the yield stress as a function of applied electric field for an STO sample with 16% water content, mixed at a concentration of 4g STO per 1ml of silicon oil. The data clearly demonstrate the importance of the boundary conditions at the electrodes, making it possible to nearly double the measured yield stress, to 210kPa at 5kV mm^{-1}, by switching from smooth electrode surfaces to electrodes covered with metal mesh. As reported before,[11] roughening the electrodes prevents slip that is likely to occur at such large shear stresses. However, to maintain a well-defined field configuration and keep the set-up as simple as possible, we present in the following data using smooth electrode surfaces. The inset to Fig.3a shows the current density *vs.* the electric field. The data roughly agrees with an exponential relationship $\ln J \sim \sqrt{E}$ also found in other GER materials,[8] which was interpreted as resulting from ionic conduction due to electric breakdown of the molecular dipoles (Poole-Frenkel effect).

The linear field response at large electric fields (>1kV mm^{-1}), a signature of the GER effect, is found not only in concentrated STO samples (Fig.3a), but persists for samples with lower water content, independent of the concentration (Fig.3b). At lower fields, however, the samples with lower water content exhibit a cross-over to a field dependence compatible with the quadratic form known for ordinary ER fluids (Fig.3b).

We find that the yield stress and the current density are directly proportional and that both depend exponentially on the water content in the particles (Fig.4). The water content was measured before mixing the sample with silicon oil, by heating to 100 °C under vacuum for 24h and looking at the weight loss. This ability to control the magnitude of the GER effect at a temperature sufficiently low to leave the STO composition intact suggests that

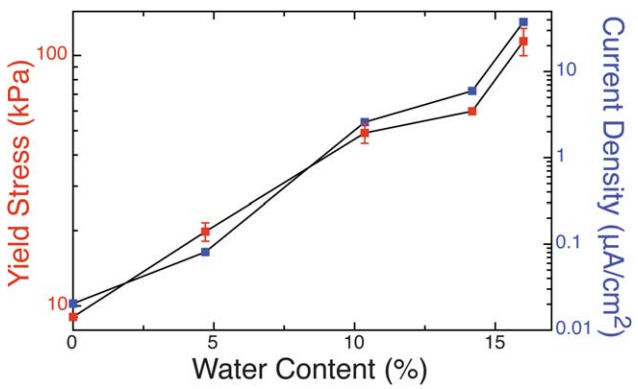

Fig. 4 Yield stress (red) and current density (blue) at 5kV mm^{-1} *vs.* water content for STO/oil 4g/ml.

† In our STO samples this maximum stress exhibits some shear rate dependence but stays within 20% of the stated value for shear rates between 10^{-3} and 10^{2} s^{-1} (see the inset to Fig. 7).

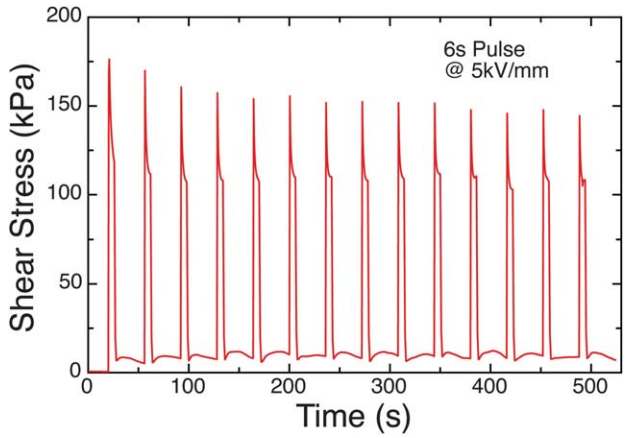

Fig. 5 Response to square pulses (5kV mm^{-1}, 6s duration) while sheared at 0.5s^{-1} (STO/oil 4g ml^{-1}; 16% water content).

our semi-crystalline STO behaves differently from the amorphous particles discussed by Lu *et al.*,[13] who reported that decreases in GER response correlated with material decomposition. Furthermore, we found that it is possible to reduce the current density by more than one order of magnitude without compromising the field effect by heating the mixed sample at 100 °C for a couple of minutes (a procedure that can be done very simply by using the heater built into the rheometer bottom plate). After drying, samples left exposed were able to recover to a certain level by grabbing moisture from the air.

In our STO samples mixed with oil the maximum water content was 16%. Above this value the current density became too high to perform measurements at high fields, and beyond 18% the mixture phase separated.

To study the dynamic response a series of square E-field pulses were applied while the sample was sheared continuously. Fig. 5 shows the shear stress response to a 6s pulse at 5kV mm^{-1} while sheared at 0.5s^{-1}. The response of the GER fluid is fast and the yield stress stays roughly constant over time. After the application of the first pulse we observe an increment in the shear stress at zero E-field. Depending on the concentration we find that the on/off shear stress ratio can reach values of 10–20 for dense suspensions and more than 500 for dilute samples.

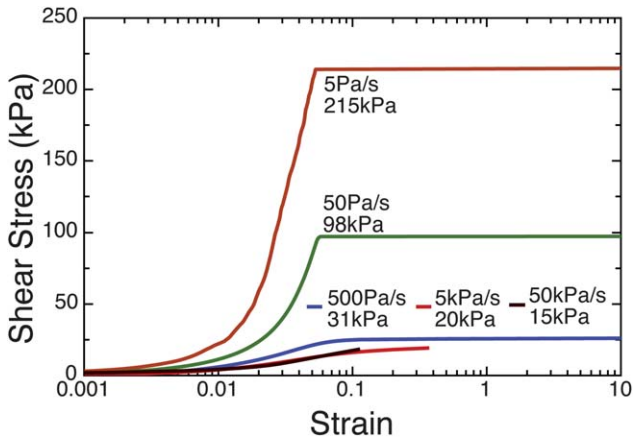

Fig. 6 Response to different rates of shear stress loading, $\dot{\tau}$, with a field of 2kV mm^{-1} applied (STO/oil 4g ml^{-1}; 16% water content). Horizontal lines indicate that the yield stress was exceeded and the sample failed abruptly.

So far, the discussion of the stress response of our STO samples concentrated on aspects qualitatively similar to that of other GER fluids reported earlier. As we show next, the dynamic response in these dense suspensions is, however, more complex than that of typical field-activated fluids.

One finding is that the yielding behavior strongly depends on the rate of which the load is applied (Fig.6). In these stress-controlled measurements a 2kV mm^{-1} field was applied with the rheometer at rest (no pre-shear applied), and then the shear stress, τ, was increased at a fixed rate, $\dot{\tau}$, while the strain was recorded. As $\dot{\tau}$ is decreased, the material becomes stiffer and exhibits abrupt failure beyond a well-defined yield stress. Unlike visco-elastic fluids, where due to the viscous contribution to the shear stress the slope of the stress-strain curve decreases with $\dot{\tau}$, the STO suspension shows an increasing slope and increasing yield stress, *i.e.*, the solid-like properties get stronger as $\dot{\tau}$ is reduced.

This is an indication of a slow structural rearrangement in response to the applied load. Such dependence on the loading history has not been reported before for this kind of fluid.

Further differences from ordinary field-activated fluids emerge in stress *versus* strain measurements performed by starting from rest and then imposing a fixed shear rate $\dot{\gamma}$ (Fig.7). A comparison of the two panels in this figure shows a strong correlation between shear and normal stresses. This starts with the overall stress magnitude and extends to details such as the phase of individual oscillations. The inset in Fig.7a shows the yield stress and the final shear stress for large strain *versus* shear rate. While the yield stress varies by no more than 10–20% (green dots) over the $\dot{\gamma}$ range 10^{-3}s^{-1}-10^{2}s^{-1} explored, the stresses observed at large strains decrease considerably (blue dots), and for large values of $\dot{\gamma}$ (100s^{-1}) the final shear stress value is close to 1kPa, which is the regular strength for common ER fluids. For the case of low shear rates the stresses can be non-monotonic, first decreasing and then increasing again ($\dot{\gamma} = 0.01$s^{-1} and below; blue traces in Fig.7a). This indicates a certain amount of healing, which goes along with the strain stiffening seen at small loading rates in Fig.6.

For the measurements shown in Fig.7 the gap separation was set to a nominal, fixed value $h = 1$mm, and the rheometer tool acted as a very stiff spring (effective spring constant $k = 1.7$MN m^{-1}). Thus, changes in measured normal force directly reflect changes in gap separation. Increases in normal stress therefore imply that the sample is dilating and expanding against the tool surface. Such dilation under shear is a clear sign that a dense STO suspension is behaving unlike an ordinary fluid and rather like a granular material.[20]

The most noticeable aspect in Fig.7 are the oscillations in both shear and normal stress. These oscillation have period 2π, *i.e.*, occur with every full rotation of the rheometer tool. With a Newtonian liquid such oscillations occur only at very small gaps and are not noticeable at the standard measuring distance of the rheometer ($h = 1$mm).‡ This is another indicator that the

‡ We checked this explicitly by using a Newtonian liquid instead of STO. Only when the gap was reduced to values of a few μm, *i.e.*, comparable to residual tilts in the tool and the bottom surfaces, did oscillations with period 2π become observable.

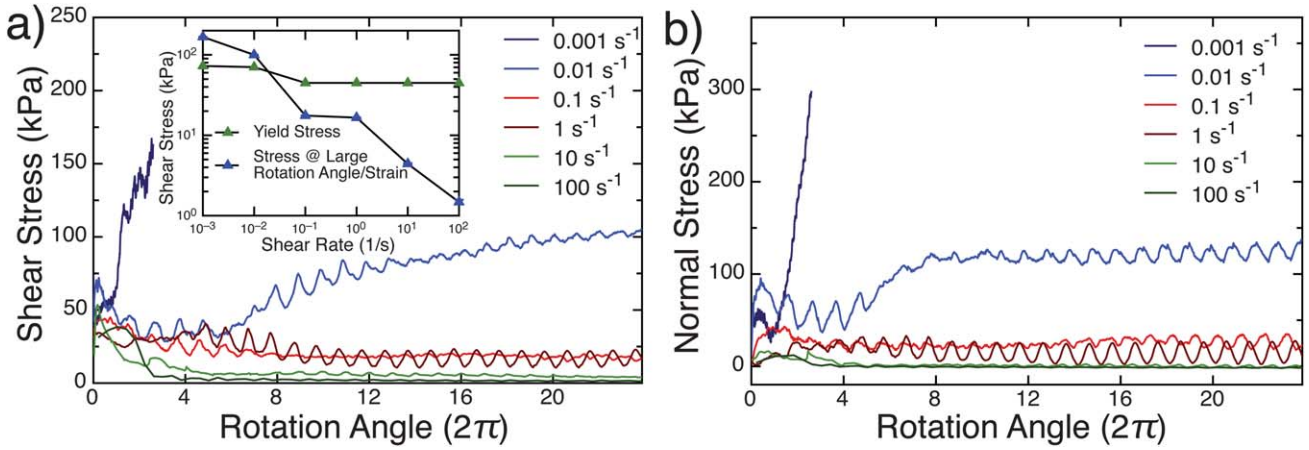

Fig. 7 Correlation between shear and normal stress response for different shear rates $\dot{\gamma}$ (STO/oil 4g ml^{-1}; 16% water content). The strain is parameterized by the rotation angle of the rheometer tool, in units of one full rotation, starting from rest. A field of 2kV mm^{-1} is applied. *a*) Shear stress. Inset: Dependence of the yield stress and the stress at large strain on shear rate. *b*) Normal stress measured simultaneously with the shear stress.

field-activated STO material behaves more solid- than liquid-like: In order to observe pronounced stress oscillations with amplitudes as large as 10–20% of the average stress, the material cannot be shearing uniformly across the 1mm gap between the electrodes; instead, the width of the actively shearing, fluid-like region must be reduced to a tiny fraction of the full gap (in the micrometre range, as we show below), with the rest of the sample effectively rigid. In other words, the large oscillations are necessarily associated with stresses being concentrated into a narrow shear band, a characteristic feature of granular material under shear.[25]

To see this, we look at what would be expected from a normal fluid confined to a gap of height h_0. Adjusting this height later to values $h_0 \ll h$ will approximate the fluid-like region inside a shear band. Oscillations with period 2π can only arise when the two bounding surfaces defining the gap are not precisely perpendicular to the rotation axis, but tilted by an angle α (see top plate on sketch in Fig.8). As the upper bounding surface moves with fixed angular speed ω set by the tool while the lower surface remains stationary, the two planes rotate in and out of alignment with period 2π in their relative azimuthal angle ϕ. Only when the two surfaces are fully aligned and thus parallel is the gap separation h_0 independent of radial, ρ, and azimuthal, θ, coordinates (we assign $\phi = 0$ to this relative orientation). In all other cases, $h_0 = h_0(\rho, \theta, \phi)$ and thus the local shear rate varies across the shearing plane.

The resulting relationship between shear stress and rotation angle ϕ can be calculated straightforwardly for a liquid of constant viscosity η subjected to a linear velocity profile between the bounding surfaces. At a given ϕ each element $dA = \rho d\rho d\theta$ of the rotating bounding surface experiences a local shear force $dF = \eta\omega\rho dA/h_0(\rho, \theta, \phi)$. This contributes a local torque $dm = \rho df = \dfrac{\eta\omega\rho^3}{h_0(\rho,\theta,\varphi)} d\rho d\theta$. From geometry we have $h(\rho,\theta,\phi) = h_0 + \Delta h\left(1 - \dfrac{\rho}{D}(\cos(\theta-\phi) + \cos\theta)\right)$, where $\Delta h = D\tan\alpha$ is the maximum amplitude of the oscillation in local gap height as the tool rotates through one full revolution.

Integration of dm over the azimuthal and radial coordinates gives the net torque on the tool, $M(\phi)$, and from this the measured shear stress $\tau(\phi) = 16M(\phi)/\pi D^3$ is obtained. Normalized by the characteristic stress scale of the system, $\tau = \eta\omega D/2h_0$, the shear stress can be expressed as

$$\frac{\tau(\phi)}{\tau} = \int_0^{2\pi} \frac{d\theta}{2\pi} \int_0^1 \frac{4\tilde{\rho}^3 d\tilde{\rho}}{1 + \varepsilon\left(1 - \tilde{\rho}\cos\left(\theta - \frac{\phi}{2}\right)\cos\frac{\phi}{2}\right)}, \qquad (1)$$

where $\tilde{\rho} = 2\rho/D$ and $\varepsilon = \Delta h/h_0$. This expression is valid for steady state shearing after the sample yielded and shows sinusoidal variations in $\tau(\phi)$, with maxima (minima) corresponding odd (even) multiples of π in rotation angle ϕ. The peak-to-peak variations normalized by the average shear stress as a function of wobble magnitude ε are plotted in Fig.8.

Fig. 8 shows that oscillation magnitudes of 10% or more of the mean shear stress require ε values of unity or larger, *i.e.*, a wobble that is of the same magnitude as the active gap h_0 itself.

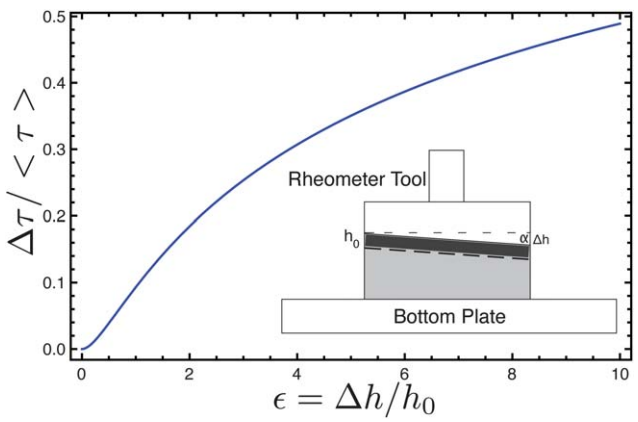

Fig. 8 Simple model for the oscillations seen in Fig.7. Main panel: Peak-to-peak variations in normalized shear stress $\Delta\tau/\langle\tau\rangle$ as a function of wobble amplitude, $\varepsilon = \Delta h/h_0$, calculated from eqn (1). Inset: Sketch of the shear band configuration. Shear is localized in the dark region.

This rules out that the GER material behaves like an ordinary liquid which shears uniformly across the full extent of the electrode gap (*i.e.*, $h_0 \approx h = 1$mm). On the other hand, already very slight tilt angles α can produce large values of ε if $h_0 \ll h$ (see sketch Fig. 8). While such shear bands could, in principle, be located anywhere inside the GER material, we find that they occur typically at the top, right underneath the rotating tool surface, while the remainder of the material remains solid-like. This is in line with experiments on a variety of granular systems which observed shear to localize near the moving boundary.[26–28] In this case a significant wobble can easily arise from a slightly tilted tool surface as it gets pressed into the paste-like GER sample before the start of the experiment. Calibration of our ER tools puts an upper limit of $\alpha < 4 \times 10^{-4}$ degrees on the tool tilt, corresponding to no more than 2-3μm for Δh. The shear stress oscillation magnitudes seen in Fig.7a therefore imply a shear band width h_0 of similar magnitude, *i.e.*, a few particle diameters across.

The frictional flow of granular systems that gives rise to dilation and shear banding also provides a natural mechanism to couple shear and normal stresses.[25] As Fig.7a demonstrates, the oscillation in normal stress are of the same order of magnitude as their shear stress counterparts and, furthermore, match their phase: at closest approach of the shearing surfaces, *i.e.*, when $\phi = \pi$ and $\tau(\phi)$ is maximum, the normal stress also peaks.

Another direct consequence of this frictional or 'granular' picture is that shear stresses can be increased significantly by counteracting the natural tendency of the material to dilate under shear. This can be done very simply by increasing the degree of confinement of the sample.[29–31] As a demonstration, we performed a set of experiments in which a non-conducting cylindrical ring around the rheometer tool was used to create lateral confinement. Fig. 9 compares stress-strain data for the different boundary conditions explored. A sufficiently large shear rate of $1s^{-1}$ was chosen so that healing of the shear band is not an issue. The weakest response (red curve) corresponds to measurements

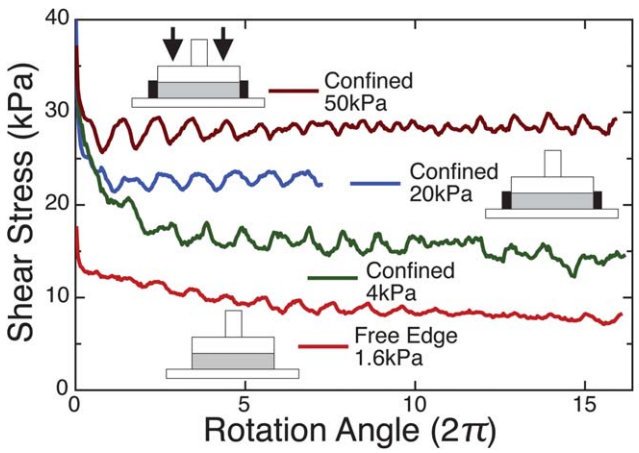

Fig. 9 Effect of confinement for different boundary conditions on shear stress *vs.* rotation angle at 2kV mm^{-1} and $\dot{\gamma} = 1s^{-1}$. Red and blue curves are in fixed gap mode, where the stress listed is the normal stress produced by dilation of the sample. Dark red and green curves are in normal force control mode (NFC) and the stress listed is the applied normal load (STO/oil 4g ml^{-1}; 14% water content).

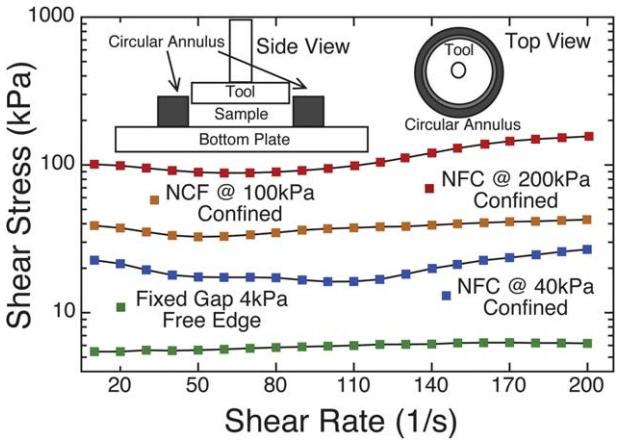

Fig. 10 Time-averaged shear stress *vs.* shear rate in the steady state at 5kV mm^{-1} for different boundary conditions and applied loads. Inset: Schematic drawing of annulus used to confine sample laterally, shown in cross-section and top view.

as shown in the previous graphs, with fixed gap but free sample edge, *i.e.*, without lateral confinement. Here the sample produces a normal stress around 1kPa and at large strains the shear stress drops to 50% of the yield stress value. Keeping the same gap settings but confining the sample laterally (blue curve) more than doubles the yield stress. The associated increase in normal stress to 20kPa indicates that the sample now dilated more in vertical direction, pushing harder against the upper electrode. Switching the rheometer from gap control mode into normal force control mode allowed us to vary the vertical confinement. Applying a normal stress of 4kPa (green curve) implies a relatively soft boundary, only slightly harder than the unconfined case. On the other hand, applying a normal stress of 50kPa exceeds the yield stress and is equivalent to strong confinement. In general, and in line with behavior expected from a granular system, the shear stress increases monotonically with normal stress, whether this is done by imposing boundary conditions similar to a stiff spring or by imposing a fixed normal load.

The effect of different boundary conditions on the steady state response is shown in Fig.10 (for 5kV mm^{-1}). As for frictional sliding, no large dependence of the shear stress on $\dot{\gamma}$ is observed. On the other hand, the key to reaching large shear stress values clearly is strong confinement and thus minimized dilation. The strongest confinement would be realized in a sealed Couette geometry, where the GER material resides in a small gap between two concentric cylinders and the field is applied across this gap. Such clutch-like sample geometry, typical for applications of field-activated fluids, was used in previous experiments on GER systems;[8,13] however, in this geometry it was not possible to measure the normal stresses at the wall.

4. Summary and conclusions

We have shown that strontium titanyl oxalate (STO) particles mixed into silicon oil exhibit a giant electrorheological (GER) effect with yield stress values at 5kV mm^{-1} up to 100 kPa for smooth electrodes and 200kPa for rough electrodes. The particle synthesis employed a new method in which STO was precipitated

out of water solution by adding alcohol. While this paper focused on highly concentrated suspensions, the GER-type field response was found to persist in more dilute suspensions, which exhibited a reduced yield stress magnitude and an increase in the *E*-field value beyond which the linear scaling starts.

Our results indicate that, at least in the STO system, a strong GER effect does not require a specially designed coating of the particles. Rather, the moisture content of the particles can be used to control the strength of the response. This implies that water molecules on the surface of the particles can take on the role of the permanent (urea) dipoles used in the barium-based GER system. Once mixed in oil, we find that the samples are stable over many months.

Investigating the dynamic response of the material, and in particular the response near yielding, we observed behavior that differs from that found in typical GER systems. Instead, the response resembles that of a much more solid-like, granular material near jamming. Manifestations of this are the observed stiffening at low shear rate, dilation under shear, and strongly correlated shear and normal stress oscillations with period of one full tool rotation. All of this supports a picture in which the sample yields by forming a narrow shear band in which the shear stress is localized while the bulk of the material remains solid-like.

A consequence of this 'granular' picture is that the overall strength of the material is controlled by the sample confinement. We demonstrated this by changing the boundary conditions. Increasing the degree of confinement makes it possible to increase the shear stress in the steady state considerably. As expected from a frictional granular system, and unlike the viscous response of normal fluids, the shear stress is largely independent of the shear rate.

5. Acknowledgements

We thank Douglas Betts, Eric Brown, Qiti Guo, Ping Sheng, Weijia Wen, Hanjun Zhang and especially Xiuqing Gong for insightful discussions. We also thank TA Instruments for supplying the thermogravimetric measurement on our particles. This work was supported by DARPA through Army grant W911NF-08-1-0209. We acknowledge use of shared experimental facilities of the Chicago Materials Research Center/MRSEC which is supported by NSF DMR-0820054.

References

1 T. C. Halsey, *Science*, 1992, **258**, 761–766.
2 T. Hao, *Adv. Mater.*, 2001, **13**, 1847–1857.
3 R. Stanway, *Mater. Sci. Technol.*, 2004, **20**, 931–939.
4 H. See, *J. Ind. Eng. Chem.*, 2004, **10**, 1132–1145.
5 W. Wen, X. Huang and P. Sheng, *Soft Matter*, 2008, **4**, 200–210.
6 W. M. Winslow, *J. Appl. Phys.*, 1949, **20**, 1137–1140.
7 H. Ma, W. Wen, W. Y. Tam and P. Sheng, *Phys. Rev. Lett.*, 1996, **77**, 2499–2502.
8 W. Wen, X. Huang, S. Yang, K. Lu and P. Sheng, *Nat. Mater.*, 2003, **2**, 727–730.
9 L. Kun-Quan, S. Rong, W. Xue-Zhao, S. Gang, W. Wei-Jia and L. Ji-Xing, *Chin. Phys.*, 2006, **15**, 2476–2480.
10 S. Chen, X. Huang, N. F. A. van der Vegt, W. Wen and P. Sheng, *Phys. Rev. Lett.*, 2010, **105**, 046001–046005.
11 R. Shen, X. Wang, Y. Lu, D. Wang, G. Sun, Z. Cao and K. Lu, *Adv. Mater.*, 2009, **21**, 4631–4635.
12 X. Gong, J. Wu, X. Huang, W. Wen and P. Sheng, *Nanotechnology*, 2010, **19**, 165602.
13 Y. Lu, R. Shen, X. Z. Wang, G. Sun and K. Q. Lu, *Smart Mater. Struct.*, 2009, **18**, 025012.
14 Y. Cheng, X. Liu, J. Guo, F. Liu, Z. Li, G. Xu and P. Cui, *Nanotechnology*, 2009, **20**, 055604.
15 X. Liu, J. Guo, Y. Cheng, G. Xu, Y. Li and P. Cui, *Rheol. Acta*, 2010, **49**, 837–843.
16 B.-X. Wang, X.-P. Zhao, Y. Zhao and C.-L. Ding, *Compos. Sci. Technol.*, 2007, **67**, 3031–3038.
17 P. Sheng, *Int. J. Mod. Phys. B*, 2005, **19**, 1157–1162.
18 X. X. Huang, W. J. Wen, S. H. Yang and P. Sheng, *Solid State Commun.*, 2006, **139**, 581–588.
19 P. Sheng and W. Wen, *Solid State Commun.*, 2010, **150**, 1023–1039.
20 A. Fall, N. Huang, F. Bertrand, G. Ovarlez and D. Bonn, *Phys. Rev. Lett.*, 2008, **100**, 018301–018305.
21 E. Brown, N. A. Forman, C. S. Orellana, H. Zhang, B. W. Maynor, D. E. Betts, J. M. DeSimone and H. M. Jaeger, *Nat. Mater.*, 2010, **9**, 220–224.
22 W. Fan and L. Niinistö, *Mater. Res. Bull.*, 1993, **29**, 451–458.
23 B. S. Patra, S. Otta and S. Bhattamisra, *Thermochim. Acta*, 2006, **441**, 84–88.
24 Z. P. Shulman, R. G. Gorodkin, E. V. Korobko and V. K. Gleb, *J. Non-Newtonian Fluid Mech.*, 1981, **8**, 29–41.
25 H. M. Jaeger, S. R. Nagel and R. P. Behringer, *Rev. Mod. Phys.*, 1996, **68**, 1259–1273.
26 C. Veje, D. W. Howell and R. Behringer, *Phys. Rev. E: Stat. Phys., Plasmas, Fluids, Relat. Interdiscip. Top.*, 1999, **59**, 739–745.
27 D. M. Mueth, G. F. Debregeas, G. S. Karczmar, P. J. Eng, S. R. Nagel and H. M. Jaeger, *Nature*, 2000, **406**, 385–389.
28 N. W. Mueggenburg, *Phys. Rev. E: Stat., Nonlinear, Soft Matter Phys.*, 2005, **71**, 031301–031310.
29 X. Tang, X. Zhang and R. Tao, *Int. J. Mod. Phys. B*, 2001, **15**, 549–556.
30 R. Tao, Y. Lan and X. Xu, *Int. J. Mod. Phys. B*, 2002, **16**, 2622–2628.
31 W. Li and X. Zhang, *Korea Aust. Rheol. J.*, 2008, **20**, 45–50.